International Journal of Nanomedicine

Dovepress
open access to scientific and medical research

Open Access Full Text Article

ORIGINAL RESEARCH

Surface modification of endovascular stents with rosuvastatin and heparin-loaded biodegradable nanofibers by electrospinning

This article was published in the following Dove Press journal:
International Journal of Nanomedicine
29 August 2017
Number of times this article has been viewed

Milka Janjic[1,2]
Foteini Pappa[1]
Varvara Karagkiozaki[1]
Christakis Gitas[2]
Kiriakos Ktenidis[2]
Stergios Logothetidis[1]

[1]Department of Physics, Laboratory for Thin Films – Nanosystems and Nanometrology, University of Thessaloniki, [2]School of Medicine, Aristotle University of Thessaloniki, Thessaloniki, Greece

Abstract: This study describes the development of drug-loaded nanofibrous scaffolds as a nanocoating for endovascular stents for the local and sustained delivery of rosuvastatin (Ros) and heparin (Hep) to injured artery walls after endovascular procedures via the electrospinning process.

Purpose: The proposed hybrid covered stents can promote re-endothelialization; improve endothelial function; reduce inflammatory reaction; inhibit neointimal hyperplasia of the injured artery wall, due to well-known pleiotropic actions of Ros; and prevent adverse events such as in-stent restenosis (ISR) and stent thrombosis (ST), through the antithrombotic action of Hep.

Methods: Biodegradable nanofibers were prepared by dissolving cellulose acetate (AC) and Ros in *N*,*N*-dimethylacetamide (DMAc) and acetone-based solvents. The polymeric solution was electrospun (e-spun) into drug-loaded AC nanofibers onto three different commercially available stents (Co–Cr stent, Ni–Ti stent, and stainless steel stent), resulting in nonwoven matrices of submicron-sized fibers. Accordingly, Hep solution was further used for fibrous coating onto the engineered Ros-loaded stent. The functional encapsulation of Ros and Hep drugs into polymeric scaffolds further underwent physicochemical analysis. Morphological characterization took place via scanning electron microscopy (SEM) and atomic force microscopy (AFM) analyses, while scaffolds' wettability properties were obtained by contact angle (CA) measurements.

Results: The morphology of the drug-loaded AC nanofibers was smooth, with an average diameter of 200–800 nm, and after CA measurement, we concluded to the superhydrophobic nature of the engineered scaffolds. In vitro release rates of the pharmaceutical drugs were determined using a high-performance liquid chromatography assay, which showed that after the initial burst, drug release was controlled slowly by the degradation of the polymeric materials.

Conclusion: These results imply that AC nanofibers encapsulated with Ros and Hep drugs have great potential in the development of endovascular grafts with anti-thrombogenic properties that can accelerate the re-endothelialization, reduce the neointimal hyperplasia and inflammatory reaction, and improve the endothelial function.

Keywords: cardiovascular disease, stent, drug delivery, scaffolds, nanocoating

Introduction

Endovascular stents have revolutionized the field of vascular surgery and have become one of the most important milestones in the treatment of a large number of vascular disorders.[1] There are different types of endovascular stents, such as bare-metal stents (BMSs), drug-eluting stents (DESs), stent grafts, and covered stents (CSs), each one with their own characteristics.[2–4] Despite their promising clinical outcome, the complications associated with their implantation still remain as a major disadvantage to their

Correspondence: Milka Janjic
Vascular Surgery Department, First Propaedeutic Surgery Clinic, AHEPA General Hospital, Aristotle University of Thessaloniki, Kiriakidi 1, GR-546 21 Thessaloniki, Greece
Tel +30 69 7734 0650
Email janjicmilka@hotmail.com

submit your manuscript | www.dovepress.com
Dovepress
http://dx.doi.org/10.2147/IJN.S138261

widespread use in percutaneous transluminal angioplasty (PTA).[5] Injury-induced neointimal hyperplasia and incomplete endothelialization of injured arteries can cause adverse events such as stent thrombosis (ST) and in-stent restenosis (ISR).[6–8] This study describes the development of a novel fiber-based hybrid rosuvastatin (Ros)–heparin (Hep)-loaded scaffold as a coating for stents for the local and sustained delivery of Ros and Hep to injured artery walls.

Statins are a class of drugs that reduce cholesterol levels by inhibiting the enzyme 3-hydroxy-3-methylglutaryl-coenzyme A (HMG-CoA) reductase, which plays a crucial role in the production of cholesterol.[9–11] Statins also exhibit non-cholesterol-dependent pleiotropic properties, inhibiting the proliferation of vascular smooth muscle cells (VSMCs) and platelet activation, improving endothelial function, and reducing inflammation.[12–14] Local delivery of statins to the diseased site via stents has the advantage of delivering high drug concentrations to the site of vascular injury, thus minimizing the possible side effects.

Hep has long been known to inhibit the proliferation of VSMCs, both in vivo and in vitro.[15,16] Several models of antiproliferative effect of Hep have been suggested, including inhibition of immediate-early genes, inhibition of production of matrix-degrading proteases, and inhibition of mitogen-activated protein kinase.[17–19] The local delivery of Hep to the site of vascular injury could be used to prevent the myeloproliferative response and acute thrombus formation, avoiding the problems of systemic drug delivery.[20] Hep encapsulation in nanofibers appears to possess the unique advantage of sustainable release, which has the benefit of sustained anticoagulation.[21]

Electrospinning is a simple and versatile method of producing ultrafine polymeric fibers with controlled surface morphology at the micro- to nanometer scale.[22] Various polymers that include synthetic, natural, and hybrid materials have been successfully electrospun (e-spun) into ultrafine fibers. The inherently high surface-to-volume ratio of fibers can enhance cell attachment, drug loading, and mass transfer properties.[26] Drugs ranging from antibiotics to anticancer agents, proteins, living cells, and various growth factors have been incorporated into e-spun fibers.[23] Among the various potential applications, the most promising is the drug delivery ability.[40] High loading capacity, high encapsulation efficiency, simultaneous delivery of diverse therapies, simplicity of operation, and cost-effectiveness are excellent features of electrospinning used in drug delivery.[24] The use of fibers as drug carriers is very promising in biomedical applications.[25,27] In this study, nonwoven fiber mats or nanoscaled cellulose acetate (AC) fibers, containing two different types of model drugs, Ros and Hep, were successfully developed and loaded on three different types of endovascular stents by the electrospinning technique.

Materials and methods

Materials

AC (M≈30,000 Da) was purchased from Sigma-Aldrich Co. (Steinheim, Germany), Ros from AstraZeneca Hellas (Athens, Greece), and Hep sodium from LEO Pharmaceutical Hellas SA (Athens, Greece). The empirical formula for Ros calcium is $(C_{22}H_{27}FN_3O_6S)_2Ca$, and the molecular weight is 1,001.14 Da. Tablets for oral administration contain 5, 10, 20, or 40 mg of Ros and the following inactive ingredients: microcrystalline cellulose national formulary (NF), lactose monohydrate NF, tribasic calcium phosphate NF, crospovidone NF, magnesium stearate NF, hypromellose NF, triacetin NF, titanium dioxide United States Pharmacopeia (USP), yellow ferric oxide, and red ferric oxide NF.

Hep sodium injection USP is a sterile, nonpyrogenic solution of Hep sodium in water for injection. Each container contains 25,000 USP Hep units; 40 or 80 mg sodium chloride added to render isotonic. The solution has pH 6.0 (5.0–7.5) and contains non-bacteriostatic, antimicrobial agent or added buffer. Hep sodium is a heterogeneous group of straight-chain anionic mucopolysaccharides called glycosaminoglycans. It is strongly acidic because of its content of covalently linked sulfate and carboxylic acid groups.

Regarding the solvents used in this study, acetone was purchased from Sigma-Aldrich Co. and *N*,*N*-dimethylacetamide (DMAc) from Chem-Lab NV (Zedelgem, Belgium), which were of analytical reagent grade and used without further purification. Phosphate-buffered saline (PBS), used in drug release kinetics studies, was also purchased by Sigma-Aldrich Co., in neutral pH. Some of the important information (ie, molecular mass, melting temperature, solubility parameter, and pK_a) of AC and the model drugs are summarized in Table 1. All the materials and reagents were used without further purification.

Table 1 Molecular mass, melting temperature, water solubility, and pK_a for AC and the model drugs

Material	Molecular mass ($g \cdot mol^{-1}$)	Melting temperature (°C)	Water solubility (mg/mL)	pK_a
AC	30.000	227–230	–	–
Ros	500.57	122	7.8	4.6
Hep sodium	12.000–15.000	<0	100.0	NA

Abbreviations: pK_a, negative base-10 logarithm of the acid dissociation constant of a solution; AC, cellulose acetate; Ros, rosuvastatin; Hep, heparin; NA, not available.

Solvent selection

In the electrospinning system, there are a number of parameters affecting fiber morphology and diameter, such as polymer concentration and viscosity, applied voltage, needle diameter, and the delivery rate of polymer solution.[25] Additionally, the solvent used to dissolve the polymer has a significant effect on the spinnability of the polymer solution and fiber morphology. In this study, DMAc and acetone (acetone/DMAc, w/v 2:1) were found as appropriate solvents for the electrospinning process and fabrication of the AC–Ros-loaded nanofibers. DMAc and acetone are organic solvents that allow full extension of the polymer, and they evaporate completely after the fiber formation process without leaving any residue on the formed fibers. The surface morphology and microstructure of the resulting composite nanofibers were characterized through scanning electron microscopy (SEM) and atomic force microscopy (AFM). The findings indicated that the diameters of the e-spun nanofibers were influenced by the concentration of AC solution, and the proper solution was found to be an important parameter affecting fiber morphology. In the nonoptimal conditions, we found that, when using different molecular weights of AC, eg, ~50,000 Da, in the electrospinning process, white deposition appeared at the bottom of the spinneret, and the electrospinning process could not be carried through. Conversely, when we used AC of $M\approx$30,000 Da, the Taylor cone at the bottom of the spinneret was clear and did not have any impurity or deposition. Therefore, AC of $M\approx$30,000 Da was selected as a proper polymer solution for electrospinning.

Solution preparation

A weighed amount of AC powder was dissolved in a mixed solution of acetone/DMAc (w/v 2:1) in order to obtain an AC solution at a concentration of 18% w/v. After that, a model drug Ros was individually added into the base AC solution under constant stirring for 24 h prior to electrospinning. The initial loading of the drugs was 100 mg, based on the weight of AC powder (2,700 mg/100 mg, w/w). Depending on the required weight to obtain the specific concentration of AC solution, different Ros tablets of 5, 10, 20, or 40 mg were powdered and added into the AC solution. Hep sodium solution was added in the original formulation with Hep of 5,000 IU/mL in solution.

Electrospinning

In this investigation, the process of the fabrication of hybrid Ros–Hep-loaded stent included two steps. In the first step, the Ros-loaded e-spun AC nanofibers were prepared by the conventional electrospinning setup via emulsion electrospinning. In the second step, the Hep solution of 5,000 IU/mL was e-spun directly onto Ros-loaded AC nanofibers with the development of Hep nanofibrous coating layer of Ros-loaded stent. In the first step, AC and Ros (2,700 mg/100 mg, w/w) in a preset weight ratio were first dissolved into 10 mL of acetone and 5 mL of DMAc, and the solution was stirred at room temperature for 24 h to obtain a uniform electrospinning solution. Three different types of commercially available stents were used: Assurant cobalt chromium stent (Medtronic Hellas, Athens, Greece), complete SE vascular nitinol stent (Medtronic Hellas), and Visi-Pro stainless steel stent system (Bard PV Hellas, Athens, Greece). All types of stents used in this experiment were in a fully expended shape during the electrospinning process. The experimental electrospinning setup contained a 5-mL standard syringe attached to a stainless steel needle with an internal diameter of 0.723 mm (21 G). The needle and the metallic pin were connected to the high-voltage supply, which produced positive direct current voltages and currents of up to 25 kV and 4.16 mA, respectively. An electric field was applied to the end of a capillary containing the polymer solution, inducing a charge on the surface of the liquid. When the voltage reached a critical value where the charge overcame the surface tension of the polymer droplet at the tip of the capillary, a jet was ejected. Acceleration through the electric field caused elongation, thinning of the polymer jet, and evaporation of the solvent to produce fibers that could be collected onto a ground plate. The solution was then e-spun using a syringe pump with a volumetric flow rate of 10.0 µL/min for 15 min to yield nanofibers on the metallic stent placed on the electrically grounded piece of aluminum foil substrate. The distance between the needle tip and the ground electrode was ~200 mm. Electrospinning process was conducted under ambient conditions. A hybrid Ros drug-loaded nanofibrous coating onto stent was formed. All manufactured stents were placed in a vacuum oven at 40°C for 72 h to evaporate the solvents. In the second step, the experimental electrospinning setup contained a 5-mL standard syringe attached to a stainless steel needle with an internal diameter of 0.405 mm (26 gage). In all, 1 mL of Hep sodium solution was added in the original formulation with Hep of 5,000 IU/mL solution. During electrospinning, 25 kV was applied at the tip of the syringe needle. The electrospinning solution flow rate was maintained at 10.0 µL/min for 15 min. E-spun nanofibers were collected on a hybrid Ros-loaded stent placed in an electrically grounded piece of aluminum foil substrate located ~150 mm below the tip of the needle. The electrospinning process was conducted at room temperature.

Morphological evaluation by SEM

Information about the surface topography and composition of samples was obtained using SEM technique (JSM-6390LV; JEOL, USA). Samples were performed using standard stabilization protocol with glutaraldehyde and ethanol, with drying of the samples at the end. Drying of the samples was made in three cycles with the addition of aqueous solutions of ethanol concentration 70%, 90% and 100% v/v sequentially. Each solution was left at samples for ~30 min. After removing the last ethanol solution, samples were allowed to dry at room conditions in a laminar flow cabinet at air atmosphere. The diameter range of the fabricated nanofibers was measured via SEM images using the image visualization software ImageJ 1.34s (National Institutes of Health, AZ, USA). Average diameter and diameter distribution were determined by measuring 100 random nanofibers from the SEM images.

Topographical evaluation by AFM

The study of topological properties of samples' surface in this experiment was performed with AFM (NTEGRA; NT-MDT, Eindhoven, the Netherlands). The software used to estimate the values of the average roughness and peak to valley was the AFM model NTEGRA and SPM (NT-MDT). Surface properties of the nanofibers were examined using a nanoscope AFM in the tapping mode and expressed as height and phase images.

Wetting behavior of samples by contact angle (CA)

Determination of hydrophilicity and hydrophobicity of AC Ros–Hep-loaded nanofibers was performed by CA. In order to measure the CAs, the mats were cut into 1 cm^2 squares and placed on a testing plate. The drop of water used for CA measurement had a volume of 5 mL, and the free surface energy of water was equal to 72.8 mN/m. The CA measurement of the samples was static and performed with a goniometer (CAM200; KSV Instruments Ltd., Helsinki, Finland). Determination of the free surface energy with the drop of deionized water was performed with the help of the Solid Free Surface Energy Calculation program. The CA measurements were made by testing the following solutions: deionized water and PBS. These solutions were used to study the behavior of materials in the various solutions that were in contact. The CA between the water droplet and the nanofibers mat was measured at various time intervals at three different locations on the sample. The average value and standard deviation (±SD) were recorded for each sample.

Biodegradation study

The biodegradability of AC drug-loaded nanofibers was studied by initial weight measures of the samples and their weight loss after specific time periods. First, the samples were cut as much as possible in the same size and placed in a 24-well plate. After that, each sample was weighed three times with an analytical balance (ABT 120-5DM; KERN & Sohn GmbH SEALED, Balingen, Germany), and then the recording of the results took place. Furthermore, 1 mL of PBS was added to each one of the samples and placed in an incubator (Galaxy 170S; New Brunswick, an Eppendorf company) at 37°C. The samples of AC drug-loaded nanofibers (4×4 cm) were weighed at 0, 3, 7, 14, 30, 45, and 60 days, and the weight loss was calculated by weight loss equation and diagrams. SEM images were taken for optical examination of the samples. The weight loss diagrams and SEM images of nanofibers were used for understanding the duration and extend of biodegradation. Finally, they were reweighed in order to see how the weight of the samples was diversified, and how the scaffolds were degraded as the days passed according to the following equation:

$$\text{Weight loss (\%)} = \frac{\text{Initial weight } (W_a) - \text{Final weight } (W_t)}{\text{Initial weight } (W_a)}$$

Here, W_a is the original weight of each sample before degradation, and W_t is the residual weight after degradation of the same samples after their complete drying.

Evaluation of drug release pharmacokinetics

The in vitro release behavior of the pharmaceuticals was determined using an elution method and a high-performance liquid chromatography assay. The scaffolds were cut into small pieces with the same shape and diameter. The pieces were then immersed in 2 mL of pre-warmed PBS, incubated at 37°C, and protected from light over a 16-day period. Thereafter, the release medium was refilled to 1.5 mL, and a sample volume of 500 µL was taken at the time points until 16 days, with replenishment of the release medium to 1.5 mL each time a sample was taken out. Time points were t=0, 2, 4, 8, 24, 96, 192, and 360 h. At each time point, 100 mL of PBS release medium was removed for sampling and replaced with fresh PBS. For each group, the assay samples were taken in triplicate (n=3) at each time interval. The amount of the drugs in the withdrawn solutions was determined using the GloMax UV luminometer from Promega Corporation (Fitchburg, WI, USA), a unique multidetection system, whereas the

absorption of the drugs was evaluated at an optical density (OD) of 240 nm wavelength for Ros and an OD of 540 nm wavelength for Hep, critical points where the drugs absorb via in vitro real-time measurements. The calibration curve for each model drug was carried out in the concentration range of 0.0025–0.05 mg/mL, in which a linear relationship between the UV absorbance and the drug concentration was realized. These data were carefully calculated to determine the cumulative amount of the drugs released from the samples at each specified immersion period. The experiments were carried out in triplicate to avoid any numerical mistake.

Results

Nanofiber morphology and structure

Nonwoven mats of submicron-sized AC fibers (M≈30,000 Da) were successfully prepared by electrospinning different concentrations (16%–20%) of AC solutions w/v in 2:1 v/v acetone/DMAc as the mixed solvent system (Table 2). The encapsulation of the functional drugs of Ros and Hep onto the fiber-based scaffolds resulted in well-formed scaffolds as shown in Figure 1, along with the mixed solvent system that was used. This mixture allowed the resulting AC solutions to be e-spun into submicron-sized cellulose fibers (200–800 nm in diameter) with pore diameters from 6 to 16 μm (Figures 2 and 3). The most red blood cells (RBCs) had diameters in the range of 6–8 μm. This indicates that the pores in the nonwoven nanofiber mats were sufficiently large to support the pass-through of RBCs in microcirculation, to provide sufficient oxygen exchange for body tissues and organs.

The solution of AC loaded with Ros and Hep drugs was e-spun into nanofibers and was mounted onto commercially available three different types of endovascular stents, Assurant cobalt stent, complete SE vascular nitinol stent, and Visi-Pro stainless steel stent system, as shown in Figure 4 for all stent materials, respectively.

Topographical evaluation by AFM

The analysis via AFM topography and morphology of the engineered scaffolds was measured in the center of each sample (tapping mode for scan sizes of 5 and 5 μm), and the images are shown in 2D in Figure 5, respectively. As we can observe from the height mode, as well as from phase AFM analysis, fiber-based structures are well formed with average roughness approaching 190 nm. Through topography characteristics, the roughness of each sample was mainly calculated from 5×5 μm images, and the results are shown in Table 3. More precisely, stents of Co–Cr with fiber scaffold deposited onto their surface exhibited an excellent distribution of the polymeric matrices, forming roughness of these structures at ~191 nm and root mean square values at 1,256.7 nm. Concerning stainless steel stents with the parallel formation of polymeric scaffolds, the roughness values slightly decreases at 186.4 nm. These results come in agreement with the other findings and lead to the conclusion that in all three samples of expertise, the topography, morphology, and roughness modifications were quite similar, in order to provide useful information for further analysis of surface parameters.

Wetting behavior of the nanofibers by CA

Hydrophilicity is an important factor in the overall performance of e-spun nanofibers. Figure 6 shows the CA measurement results for stable water droplets placed on the nanofiber mats. The final CAs of 14%, 15%, 16%, 17%, and 18% AC Ros–Hep-loaded nanofibers were 9.66±3.36, 46.96±0.43, 44.11±11.27, 32.28±3.38, and 20.97±2.19, respectively. The addition of Hep reduced the CA, and additionally, the incorporation of Ros and Hep slightly improved the hydrophilicity of the nanofiber because of the larger number of hydrophilic proteins on or near the fiber surface.

The results are presented in Table 4. The 14% AC drug-loaded nanofibers had the most hydrophilic surface

Table 2 Electrospinning deposition results for different concentrations of AC (M≈30,000 Da)

Solvents (2:1)	Concentration (%)	Voltage	Speed	Distance	Needle	Syringe	Pattern	Fibers
Acetone/DMAc	16	25	10	200	21 G	1	Biospiral	Fibers
Acetone/DMAc	16	25	10	200	24 G	1	Biospiral	Fibers
Acetone/DMAc	20	25	10	200	21 G	1	Biospiral	Fibers
Acetone/DMAc	20	25	10	200	24 G	1	Biospiral	Fibers
Acetone/DMAc	16	25	10	200	21 G	2	Biospiral	Fibers
Acetone/DMAc	16	25	10	200	24 G	2	Biospiral	Fibers
Acetone/DMAc	17	25	10	200	21 G	1	Biospiral	Fibers
Acetone/DMAc	18	25	10	200	21 G	1	Biospiral	Fibers
Acetone/DMAc	19	25	10	200	21 G	1	Biospiral	Fibers

Abbreviations: AC, cellulose acetate; DMAc, *N*,*N*-dimethylacetamide; G, gage.

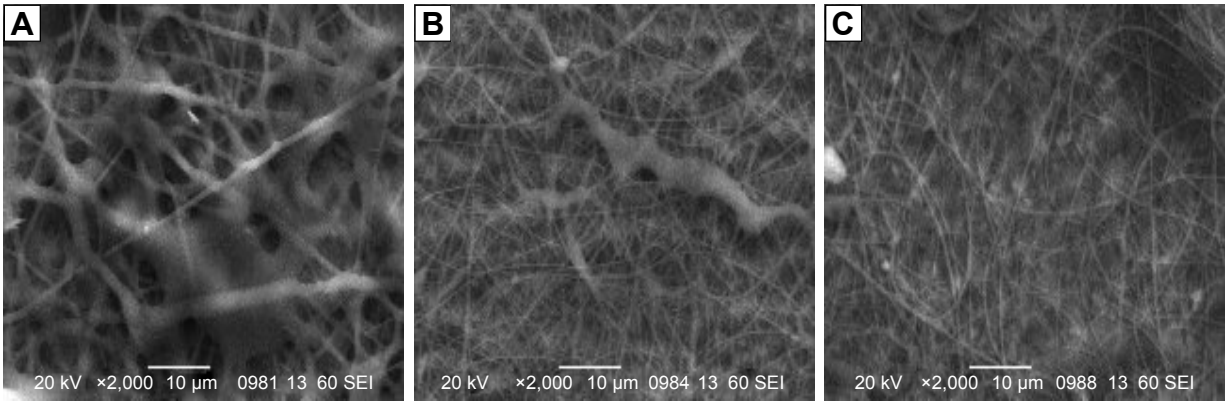

Figure 1 SEM images of (**A**) AC nanofibers, (**B**) AC nanofibers loaded with Ros, and (**C**) AC nanofibers loaded with Ros and Hep.
Note: Scale bar: 10 µm.
Abbreviations: SEM, scanning electron microscopy; AC, cellulose acetate; Ros, rosuvastatin; Hep, heparin.

compared with other drug-loaded matrices. Generally, all samples exhibited hydrophilic behavior, with 14% and 18% AC Ros–Hep-loaded nanofibers having the most hydrophilic surface. Using the CA measurements of the samples, another significant parameter was calculated, the free surface energy. There is an inverse relationship between CA and free surface energy (Table 4). With the increase in CA, there is a reduction in free surface energy and hence the ability of the sample to interact with polar solvents. After analyzing different parameters, we chose for our study the 18% AC Ros–Hep-loaded nanofibers, in order to develop hybrid CS, due to their best performance.

Biodegradation study results

In vitro degradation of nonwoven fibers of a biodegradable AC scaffold is shown at the comparison diagrams (Figure 7).

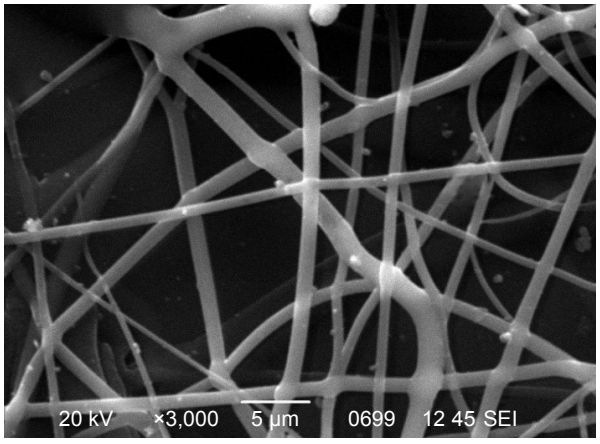

Figure 2 Morphology of nanofibrous membrane by SEM.
Note: Ros–Hep-loaded AC nanofibers with diameters from 200 to 800 nm and pore diameters from ~6 to ~16 µm (scale bar: 5 µm).
Abbreviations: SEM, scanning electron microscopy; Ros, rosuvastatin; Hep, heparin; AC, cellulose acetate.

With the SEM micrographs, the changes in the molecular weight of the polymer are better distinguished by demonstrating how the polymer is degraded in 3, 30, and 60 days (Figure 7). As noted via ImageJ software, from day 3 to 30, a mass raise took place due to fibers' swelling, which led to an increase in the diameter of fibers, and from day 30 to 60, a decrease in the diameter of fibers, as expected, because of melting of fibers and polymer degradation.

In vitro drug release profile of pharmaceuticals

The daily and accumulative release curves of Ros and Hep from the nanofibers are plotted in Figures 8–11. Diagrams shown in Figures 8 and 10 are representative of ones from the reference curves of Ros and Hep accordingly. The measurements suggest that some of pharmaceuticals were presented on the surface of the nanofibers, inducing the initial burst of drug release (Figures 9 and 11). However, most pharmaceuticals were dispersed in the bulk of the AC matrix, inducing stable drug release. Following the initial burst release, the drug release followed a controlled, solely release by degradation of the polymeric materials (Figures 9 and 11). The hybrid DESs that were developed herein provided local and sustained delivery of high concentrations of Ros and Hep for 4 weeks. Delivering high concentrations of Ros and Hep to arterial wall using proposed hybrid DES may represent a superior and novel therapeutic method for patients who have a high risk of ST and minimize possible systemic side effects.

Discussion

Despite the major advances in vascular stent technology, many issues such as acute or late ST and ISR after the successful

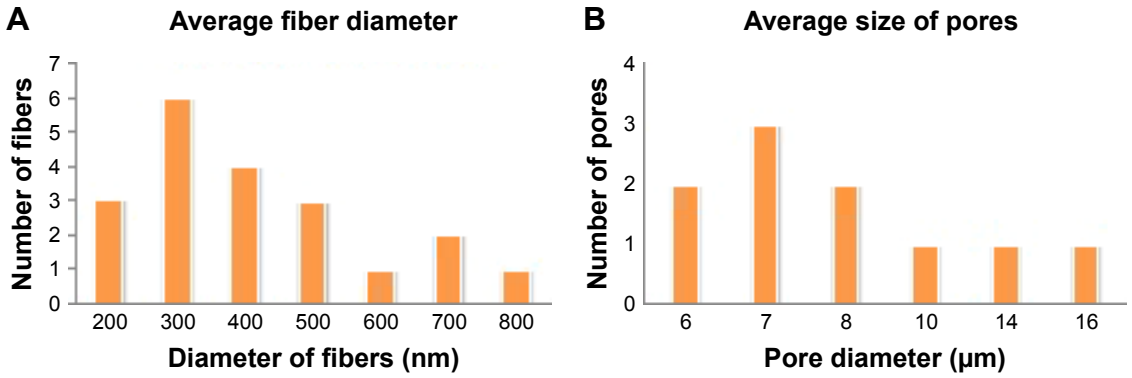

Figure 3 Diagrams of (**A**) diameter of e-spun nanofibers (nm) and (**B**) pore diameter (μm).
Note: Ros–Hep-loaded AC nanofibers with diameters from 200 to 800 nm and pore diameters from ~6 to ~16 μm.
Abbreviations: e-spun, electrospun; Ros, rosuvastatin; Hep, heparin; AC, cellulose acetate.

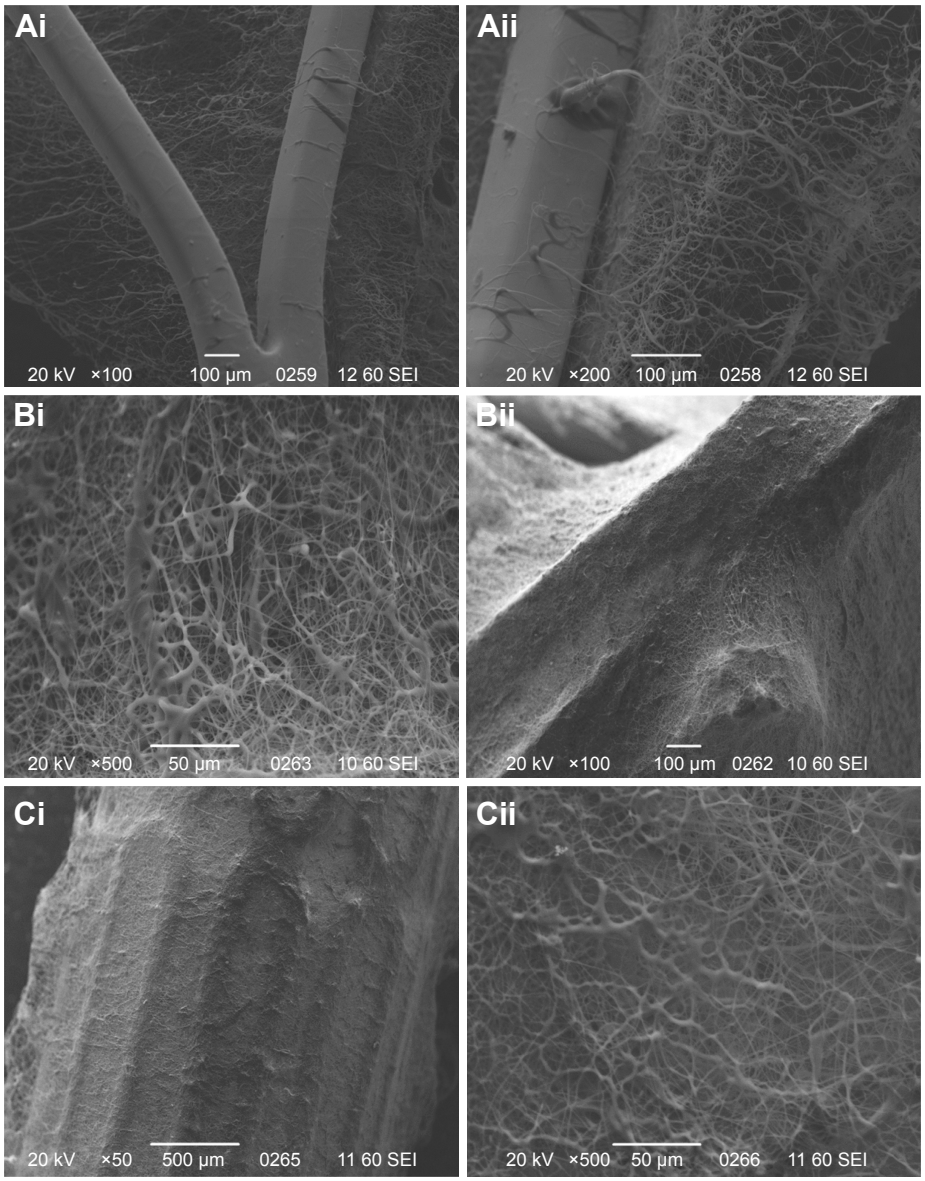

Figure 4 SEM images of (**Ai**) Ni–Ti stent with nanofibers, (**Bi**) stainless steel stent with nanofibers, and (**Ci**) Co–Cr stent with nanofibers.
Note: (**Aii**–**Cii**) are magnified images of (**Ai**–**Ci**).
Abbreviations: SEM, scanning electron microscopy; Ni–Ti, nickel–titanium alloy stent; Co–Cr, cobalt–chromium alloy stent.

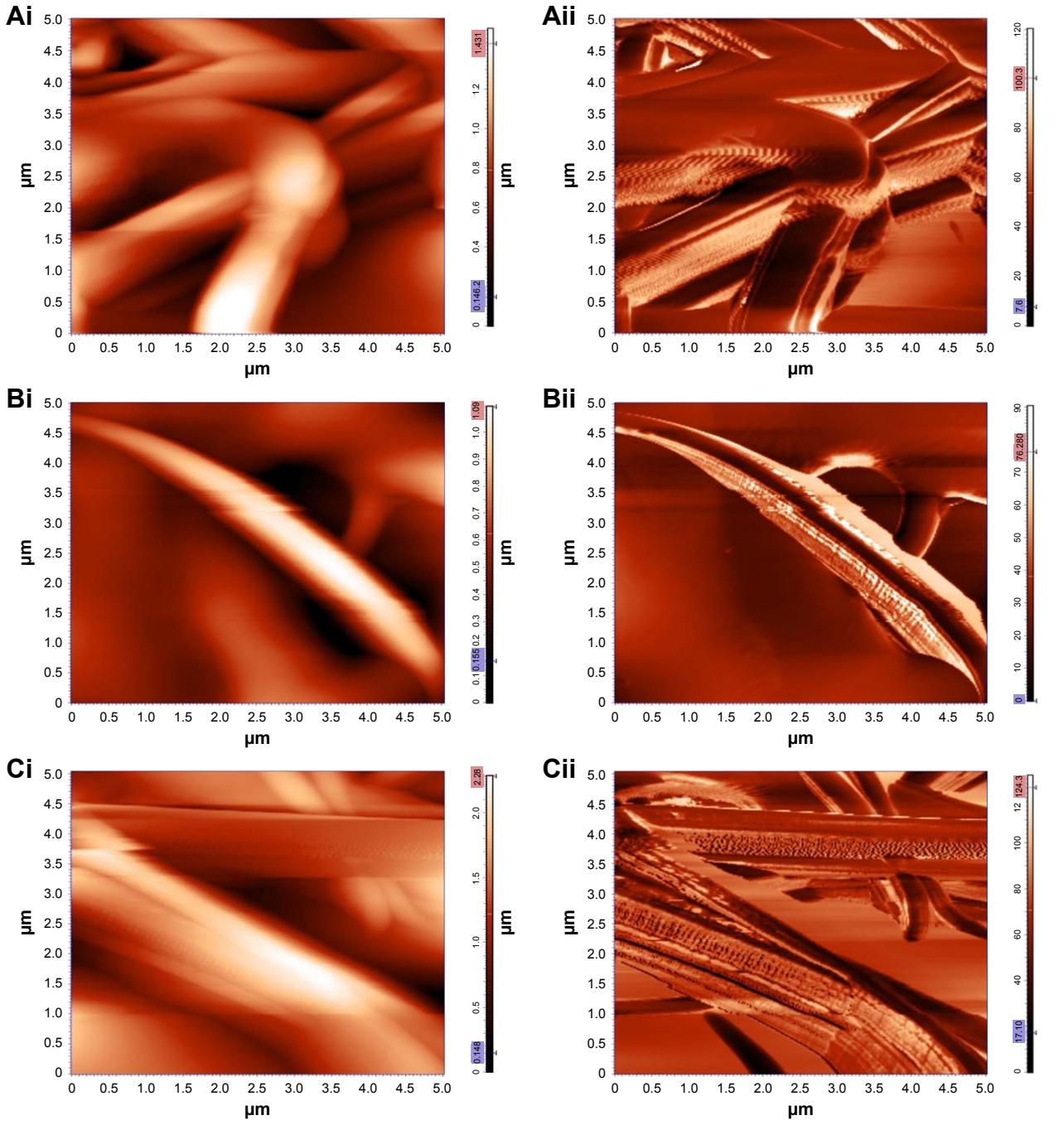

Figure 5 AFM images of thin films (10×10 µm).
Notes: (**Ai**) Co–Cr, (**Bi**) Ni–Ti, and (**Ci**) stainless steel. (**Ai–Ci**): topography and (**Aii–Cii**): phase.
Abbreviations: AFM, atomic force microscopy; Co–Cr, cobalt–chromium alloy stent; Ni–Ti, nickel–titanium alloy stent.

Table 3 Topography and roughness analysis via AFM tools of the stent samples

Groups	Root mean square (nm)	Peak to valley (nm)
Co–Cr	1,256.7	191.2
Ni–Ti	1,232.1	178.42
Stainless steel	1,408.7	186.4

Abbreviations: AFM, atomic force microscopy; Co–Cr, cobalt–chromium alloy stent; Ni–Ti, nickel–titanium alloy stent.

endovascular procedures still remain unresolved.[6–8] A healthy endothelial layer provides homeostatic control, and the adhesion of endothelial cells on the stent surface after the endovascular procedures is the key for the repair of vascular injury, preventing thrombosis and proliferation of smooth muscle cells (SMCs). Injury-induced migration and proliferation of SMCs remain the major pathophysiological

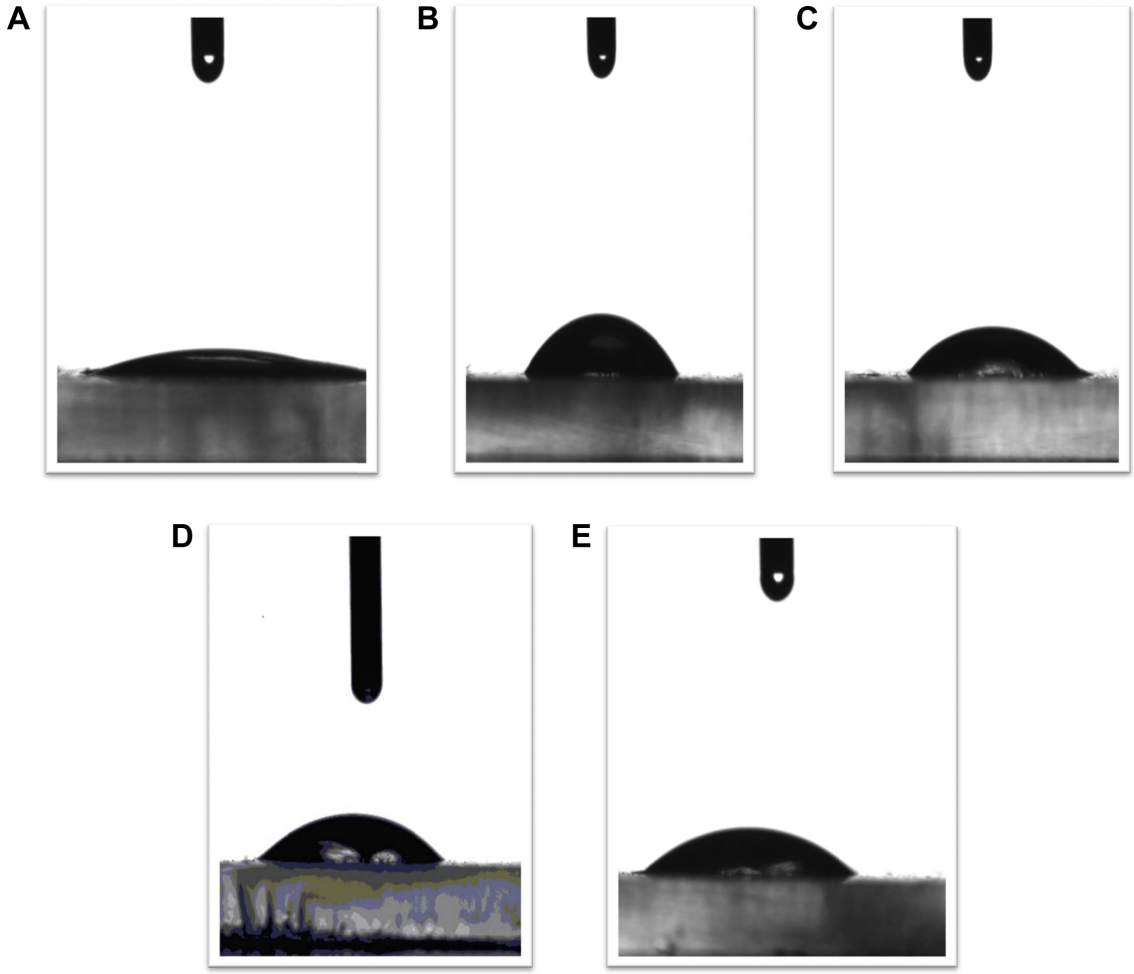

Figure 6 Determination of the wetting behavior of AC Ros–Hep-loaded nanofibers via CA measurement in concentrations of (**A**) 14%, (**B**) 15%, (**C**) 16%, (**D**) 17%, and (**E**) 18%.
Note: 14%, 15%, 16%, 17%, and 18% are different concentrations of AC drug-loaded nanofibers.
Abbreviations: AC, cellulose acetate; Ros, rosuvastatin; Hep, heparin; CA, contact angle.

causes of neointimal hyperplasia and subsequent ISR.[35–38] The complications associated with BMSs and the first- and second-generation DESs have led to the development of next-generation stent systems, called CSs.[34,35,46,47] CSs obtain a thin membrane that either covers the interior lumen or the adluminal surface of the metallic stent scaffold or completely covers the stent in a sandwich-like configuration. They can act as effective drug delivery platforms for local and sustained release of therapeutic agents and can be modified with anticoagulants and antiproliferative and immunosuppressant agents. Drug incorporation and delivery is one of the crucial characteristics for current stenting systems.[33] However, compared to the conventional DESs, nanocoated CSs for the local and sustained drug delivery in atherosclerotic disease have received little attention. One of the main areas of research in nanomedicine is the drug delivery systems where the e-spun nanofibers help to encapsulate the therapeutic agent in the fibers. Owing to the mild processing parameters, fibers maintain the bioactivity and robustness of the drug molecules and their localized inoculation and can

Table 4 Determination of the hydrophilicity/hydrophobicity of AC nanofibers with the technique of CA measurement in concentrations of 14%, 15%, 16%, 17%, and 18%

Scaffolds (%)	CA (degree)	Free surface energy γ_{sv} (mN/m)
14	9.66±3.36	5.12
15	46.96±0.43	4.97±0.04
16	44.11±11.27	8.55±5.58
17	32.28±3.38	6.86
18	20.97±2.19	5.99

Note: 14%, 15%, 16%, 17%, and 18% are different concentrations of AC drug-loaded nanofibers.
Abbreviations: AC, cellulose acetate; CA, contact angle.

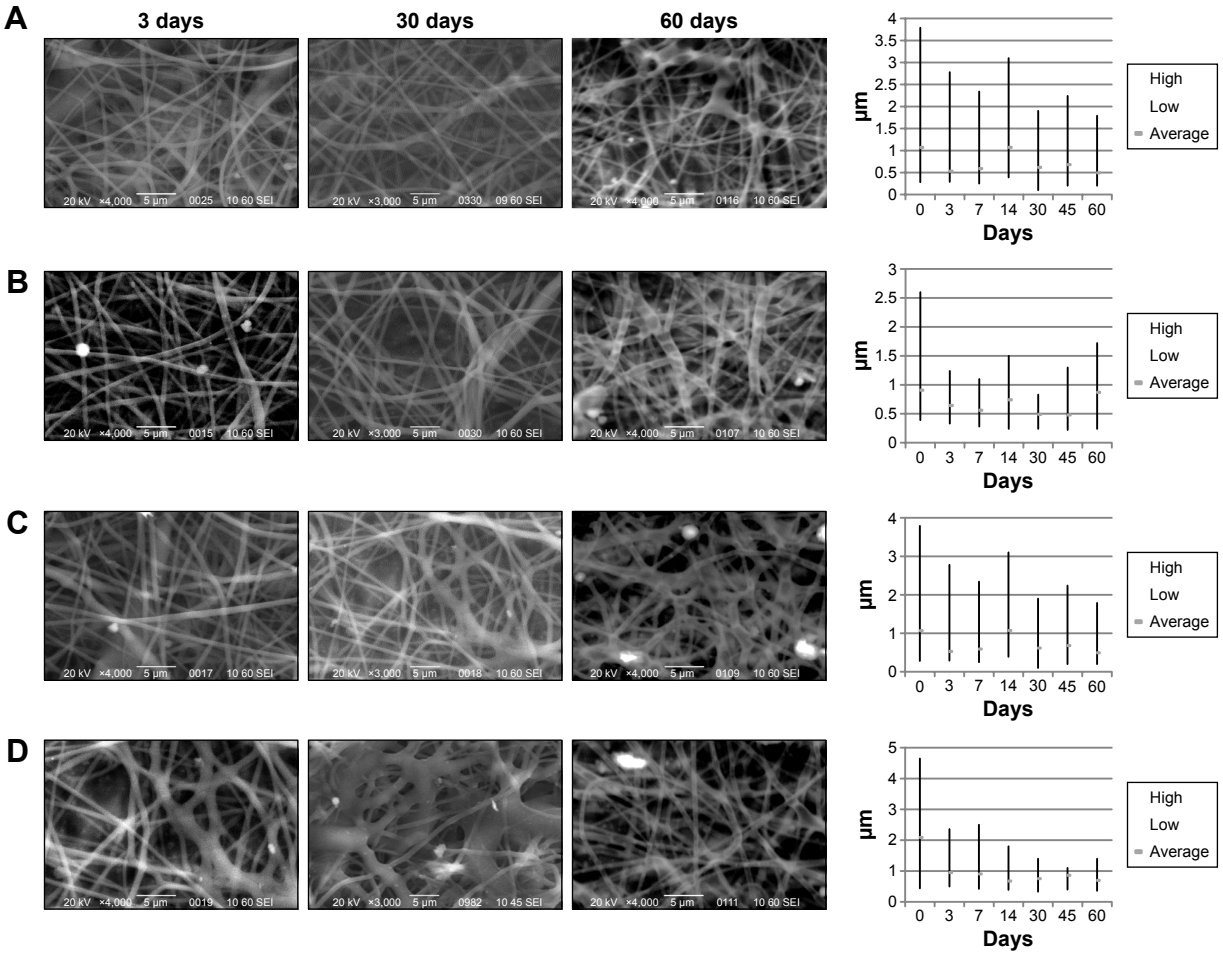

Figure 7 SEM images and diagrams of biodegradation of (**A**) 14%, (**B**) 16%, (**C**) 18%, and (**D**) 20% AC drug-loaded nanofibers at 3, 30, and 60 days.
Note: 14%, 16%, 18%, and 20% are different concentrations of AC drug-loaded nanofibers.
Abbreviations: SEM, scanning electron microscopy; AC, cellulose acetate.

significantly reduce the systemic absorption of the drug, thus preventing or reducing drug side effects. In addition, the efficacy of the drug is improved due to target treatment localization.[41] Drug release pharmacokinetics is dependent on the degradation of polymer fibers and thus can be properly managed by controlling the process of encapsulation and the architecture of nanofibers.[28–30,39]

In this study, we used AC polymer to develop nonwoven matrices of submicron-sized cellulose fibers to overcome safety issues, such as inflammation induced by the durable

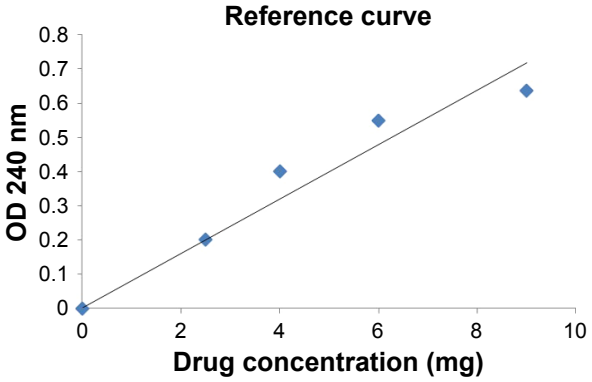

Figure 8 Reference curve of Ros drug for different concentrations along with OD measurements.
Abbreviations: OD, optical density; Ros, rosuvastatin.

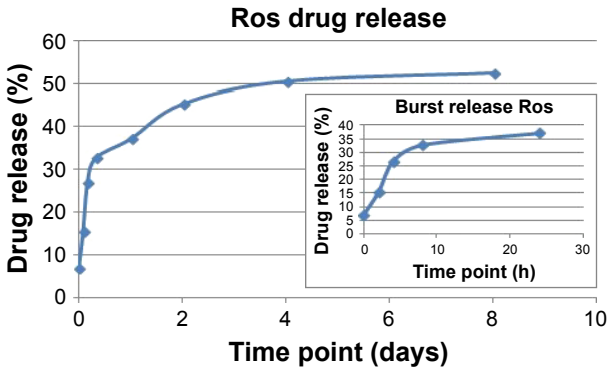

Figure 9 Ros release pharmacokinetics along with burst release of the drug in the index.
Abbreviation: Ros, rosuvastatin.

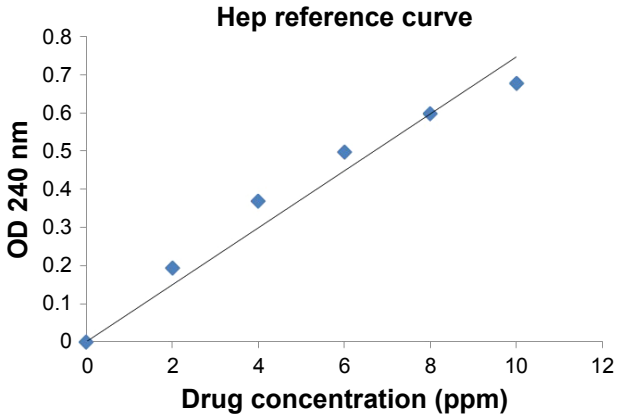

Figure 10 Reference curve of Hep drug for different concentrations along with OD measurements.
Abbreviations: Hep, heparin; OD, optical density.

polymers and polymer hypersensitivity and toxicity due to the good biocompatibility and biodegradability of AC polymer. In vitro biodegradation study results showed the degradation of nonwoven fibers of biodegradable AC scaffolds over 60 days. The changes in the molecular weight of the polymers from day 3 to 30 with mass raise took place due to fibers' swelling, which led to an increase in the diameter of fibers, and from day 30 to 60, a decrease in the diameter of fibers took place, as expected, because of melting of fibers and polymer degradation. The nanofibers protect the encapsulated drug and prevent other molecules from denaturing during processing.[39,42,43] Thus, the therapeutic agents remain invariable until they reach the site of activity. Many compounds for therapeutic use can be encapsulated within the nanofibers for drug delivery.[31,32] The high surface area of the nanofibers defeats the loading limitations that come across in usual drug delivery methods. The surface area of the nanofibers can be further increased by creating pores on nanofibers.[42,44] Pores increase the surface area and additionally provide a larger number of binding sites for drug loading. These pores can be created by the selective removal of materials or by modifying the electrospinning techniques.[42,44] Drug release pharmacokinetics can be controlled by varying the electrospinning parameters such as the mesh size and fiber diameter.[45]

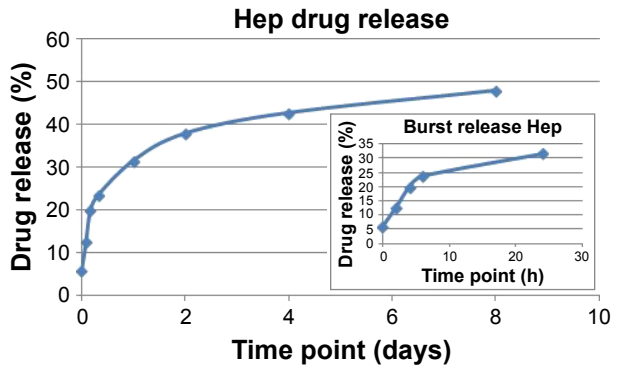

Figure 11 Hep release pharmacokinetics along with burst release of the drug in the index.
Abbreviation: Hep, heparin.

The therapeutic compounds can be encapsulated in nanofibers using two different techniques. The simplest technique is by blending, whereby the drug molecules are mixed with the polymer and e-spun together to form nanofibers. The fibers with a larger diameter showed zero-order kinetics in drug release, which means that the rate of drug release is constant.[44] In this technique, the molecules are located on the surface of the fibers and the process is easy to perform. The second technique used to create encapsulated drug delivery systems is the core–shell structure using the coaxial spinneret; the drug is released with an initial burst and then stabilizes to a constant release rate.[45] In addition, the therapeutic compounds can be coated on the surface of the fibers. In this method, the drug molecules can be adsorbed or cross-linked to the fibers via physical and chemical bonds.[39]

As described in the aforementioned experiments, we successfully developed a hybrid Ros–Hep-loaded fibrous-based nanocoating stent via a two-step process.[22,23] In the first step, the Ros-loaded AC nanofibers were prepared by the conventional electrospinning setup via emulsion electrospinning. In the second step, the Hep solution of 5,000 IU/mL was e-spun directly onto Ros-loaded AC nanofibers with the development of Hep nanofibrous coating layer of Ros-loaded stent. Delivering high concentrations of Ros and Hep to arterial walls using the hybrid DES may constitute an ideal therapeutic method for patients who have a high risk of ST and ISR and minimize possible side effects.[20] Numerous non-lipid modifiable effects of statins designate as pleiotropic effects could be beneficial for the treatment of various severe disorders. Over the past 15 years, several clinical trials indicated that the benefits of statins extend beyond their effects on cholesterol and suggested the involvement of mechanisms other than lipid-lowering activity.[48,49] Besides the many others, the most important pleiotropic effects of statins are anti-inflammatory, antiproliferative, antioxidant, immunomodulatory, neuroprotective, and antithrombotic effects; improved endothelial dysfunction; and impaired vascular remodeling.[48] The retrospective studies that assess the effect of statin therapy on restenosis after percutaneous transluminal coronary angioplasty (PTCA) show that statin therapy was associated with a remarkably improved survival free of myocardial infarction (MI) and with a significant

reduction in repeat target vessel revascularization (TVR) during 6-month follow-up. Minimal lumen diameter was significantly larger, late lumen loss and restenosis rates were significantly lower, and clear benefit in patients receiving statin therapy was significantly increased compared with the no-statin group.[51] An intravascular study clearly described that aggressive lipid-lowering therapy with atorvastatin for 1 year inhibited plaque growth of minor lesions. Other multivariate analysis identified that statin therapy was associated with a remarkable reduction in acute or late ST, ISR, and TVR after the successful endovascular procedures.[51] Our results imply that e-spun AC nanofibers containing Ros and Hep have great potential in the development of vascular grafts with anti-thrombogenic properties, which can accelerate the re-endothelialization, reduce the neointimal hyperplasia and inflammatory reaction, and improve the endothelial function. The pleiotropic effects of statins are under continuous investigation to entirely establish their role in the prevention of vascular and cardiovascular events. The results of several ongoing clinical trials aimed more specifically at pleiotropic effects of statins and their relative clinical relevance and importance.[50] In addition, Hep has long been known to inhibit the proliferation of VSMCs both in vivo and in vitro.[15,16] Several models of antiproliferative effect of Hep have been suggested, including inhibition of immediate-early genes, inhibition of production of matrix-degrading proteases, and inhibition of mitogen-activated protein kinase.[17–19] The local delivery of Hep to the site of vascular injury could be used to inhibit the proliferation of VSMCs and acute thrombus formation, avoiding systemic drug delivery problems.[20] Hep encapsulated in the nanofibers could be released sustainably, with the benefit of sustained anticoagulation.[21]

Conclusion

Surface properties of endovascular stents materials play an important role in determining adhesion behaviors of endothelial cells and blood platelets. Owing to the complex mechanism of ISR, sole surface modification of endovascular devices is hard to completely prevent ISR or ST. However, combined with other techniques, such as drug delivery or cell seeding and related adjuvant therapy, it could inhibit determining factors of ISR, including inflammation, proliferation of SMCs, and thrombosis, and eventually prevent ISR. To investigate the appropriate choice of loading method, drug dosage and release kinetics, drug biodistribution, possible side effects, and metabolism of the carrier polymers, further in vivo studies are needed in order to provide the base for their commercialization and future clinical usage.

Disclosure

The authors report no conflicts of interest in this work.

References

1. Sigwart U, Puel J, Mirkovitch V, Joffre F, Kappenberger L. Intravascular stents to prevent occlusion and restenosis after transluminal angioplasty. *N Engl J Med*. 1987;316(12):701–706.
2. Mani G, Feldman MD, Patel D, Agrawal CM. Coronary stents: a materials perspective. *Biomaterials*. 2007;28(9):1689–1710.
3. Kabir AM, Selvarajah A, Seifalian AM. How safe and how good are drug-eluting stents? *Future Cardiol*. 2011;7(2):251–270.
4. Morice MC, Serruys PW, Barragan P, et al. Long-term clinical outcomes with sirolimus-eluting coronary stents: five-year results of the RAVEL trial. *J Am Coll Cardiol*. 2007;50(14):1299–1304.
5. Farhatnia Y, Tan A, Motiwala A, Cousins BG, Seifalian AM. Evolution of covered stents in the contemporary era: clinical application, materials and manufacturing strategies using nanotechnology. *Biotechnol Adv*. 2013;31(5):524–542.
6. Inoue T, Node K. Molecular basis of restenosis and novel issues of drug-eluting stents. *Circ J*. 2009;73(4):615–621.
7. Hamid H, Coltart J. "Miracle stents" – a future without restenosis. *Mcgill J Med*. 2007;10(2):105–111.
8. Waltham M, Harris J. Intimal hyperplasia: the nemesis of cardiovascular intervention. *ANZ J Surg*. 2004;74(9):719–720.
9. Rosenson RS. Rosuvastatin: a new inhibitor of HMG-coA reductase for the treatment of dyslipidemia. *Expert Rev Cardiovasc Ther*. 2003;1(4):495–505.
10. McKenney JM. Efficacy and safety of rosuvastatin in treatment of dyslipidemia. *Am J Health Syst Pharm*. 2005;62(10):1033–1047.
11. Chapman MJ, McTaggart F. Optimizing the pharmacology of statins: characteristics of rosuvastatin. *Atheroscler Suppl*. 2002;2(4):33–37.
12. Kinlay S, Schwartz GG, Olsson AG, et al. High-dose atorvastatin enhances the decline in inflammatory markers in patients with acute coronary syndromes in the MIRACL study. *Circulation*. 2003;108(13):1560–1566.
13. Zago AC, Matte BS, Reginato L, et al. First-in-man study of simvastatin-eluting stent in de novo coronary lesions: the SIMVASTENT study. *Circ J*. 2012;76(5):1109–1114.
14. Miyauchi K, Kasai T, Yokayama T, et al. Effectiveness of statin-eluting stent on early inflammatory response and neointimal thickness in a porcine coronary model. *Circ J*. 2008;72(5):832–838.
15. Clowes AW, Karnowsky MJ. Suppression by heparin of smooth-muscle cell-proliferation in injured arteries. *Nature*. 1977;265(5595):625–626.
16. Hoover RL, Rosenberg R, Haering W, Karnovsky MJ. Inhibition of rat arterial smooth muscle cell proliferation by heparin II. In vitro studies. *Circ Res*. 1980;47(4):578–583.
17. Pukac LA, Castellot JJ Jr, Wright TC Jr, Caleb BL, Karnovsky MJ. Heparin inhibits c-fos and c-myc mRNA expression in vascular smooth muscle cells. *Cell Regul*. 1990;1(5):435–443.
18. Kenagy RD, Nikkari ST, Welgus HG, et al. Heparin inhibits the induction of 3 matrix metalloproteinases (stromelysin, 92-kD gelatinase, and collagenase) in primate arterial smooth-muscle cells. *J Clin Invest*. 1994;93(5):1987–1993.
19. Mishra-Gorur K, Castellot JJ. Heparin rapidly and selectively regulates protein tyrosine phosphorylation in vascular smooth muscle cells. *J Cell Physiol*. 1999;178(2):205–215.
20. Wang B, Wang Y, Yin T, et al. Applications of electrospinning technique in drug delivery. *Chem Eng Commun*. 2010;197:1315–1338.
21. Su Y, Li X, Liu Y, et al. Encapsulation and controlled release of heparin from electrospun poly (L-lactide-co-epsilon-caprolactone) nanofibers. *J Biomater Sci Polym Ed*. 2010;22(1–3):165–177.
22. Chakraborty S, Liao IC, Adler A, Leong KW. Electro hydrodynamics: a facile technique to fabricate drug delivery systems. *Adv Drug Deliv Rev*. 2009;61(12):1043–1054.

23. Liu S, Zhou G, Liu D, et al. Inhibition of orthotopic secondary hepatic carcinoma in mice by doxorubicin-loaded electrospun polylactide nanofibers. *J Mater Chem B*. 2013;1:101–109.
24. Zamani M, Prabhakaran MP, Ramakrishna S. Advances in drug delivery via electrospun and electrosprayed nanomaterials. *Int J Nanomedicine*. 2013;8:2997–3017.
25. Pham QP, Sharma U, Mikos AG. Electrospinning of polymeric nanofibers for tissue engineering applications: a review. *Tissue Eng*. 2006; 12(5):1197–1211.
26. Heydarkhan-Hagvall S, Schenke-Layland K, Dhanasopon AP, et al. Three-dimensional electrospun ECM-based hybrid scaffolds for cardiovascular tissue engineering. *Biomaterials*. 2008;29(19):2907–2914.
27. Karagkiozaki V, Loogothetidis S, Pappa AM. Nanomedicine for atherosclerosis: molecular imaging and treatment. *J Biomed Nanotechnol*. 2015;11(2):191–210.
28. Chen X, Liu Y, Miao L, et al. Controlled release of recombinant human cementum protein 1 from electrospun multiphasic scaffold for cementum regeneration. *Int J Nanomedicine*. 2016;11:3145–3158.
29. Mei L, Wang YL, Tong AP, Guo G. Facile electrospinning of an efficient drug delivery. *Expert Opin Drug Deliv*. 2016;25:1–13.
30. Hsu YH, Lin CT, Yu YH, Chou YC, Liu SJ, Chan EC. Dual delivery of active antibactericidal agents and bone morphogenetic protein at sustainable high concentrations using biodegradable sheath-core-structured drug-eluting nanofibers. *Int J Nanomedicine*. 2016;11:3927–3937.
31. Guo G, Fu SZ, Zhou LX, et al. Preparation of curcumin loaded poly(ε-caprolactone)-poly(ethylene glycol)-poly(ε-caprolactone) nanofibers and their in vitro antitumor activity against Glioma 9L cells. *Nanoscale*. 2011;3(9):3825–3832.
32. Zhou YY, Yao HC, Wang JS, Wang DL, Liu Q, Li ZJ. Greener synthesis of electrospun collagen/hydroxyapatite composite fibers with an excellent microstructure for bone tissue engineering. *Int J Nanomedicine*. 2015;10:3203–3215.
33. Joner M, Finn AV, Farb A, et al. Pathology of drug-eluting stents in humans: delayed healing and late thrombotic risk. *J Am Coll Cardiol*. 2006;48(1):193–202.
34. Radeleff B, Lopez-Benitez R, Stampfl U, et al. Paclitaxel-induced arterial wall toxicity and inflammation: tissue uptake in various dose densities in a minipig model. *J Vasc Interv Radiol*. 2010;21(8):1262–1270.
35. Dzau VJ, Braun-Dullaeus RC, Sedding DG, et al. Vascular proliferation and atherosclerosis: new perspectives and therapeutic strategies. *Nat Med*. 2002;8(11):1249–1256.
36. Gibbons GH, Dzau VJ. The emerging concept of vascular remodeling. *N Engl J Med*. 1994;330(20):1431–1438.
37. Doran AC, Meller N, McNamara CA. Role of smooth muscle cells in the initiation and early progression of atherosclerosis. *Arterioscler Thromb Vasc Biol*. 2008;28(5):812–819.
38. Newby AC. Dual role of matrix metalloproteinases (matrixins) in intimal thickening and atherosclerotic plaque rupture. *Physiol Rev*. 2005;85(1):1–31.
39. Chen F, Huang P, Mo X. Electrospinning of heparin encapsulated P (LLA-CL) core/shell nanofibers. *Nano Biomed Eng*. 2010;2:56–60.
40. Cui W, Zhou Y, Chang J. Electrospun nanofibrous materials for tissue engineering and drug delivery. *Sci Tech Adv Mat*. 2010;11(1): 014108.
41. Wanga B, Wanga Y, Yina T, et al. Applications of electrospinning techniques drug delivery. *Chem Eng Commun*. 2010;197(10):1315–1338.
42. Okudaa T, Tominagab K, Kidoaki S. Time-programmed dual release formulation by multilayered drug-loaded nanofiber meshes. *J Control Release*. 2010;143(2):258–264.
43. Pratyush D, Jing L, Satish K, et al. Experimental and theoretical investigations of porous structure formation in electrospun fibers. *Macromolecules*. 2007;40(21):7689–7694.
44. Cui W, Li X, Zhu X, Yu G, Zhou S, Weng J. Investigation of drug release and matrix degradation of electrospun poly(DL-lactide) fibers with paracetanol inoculation. *Biomacromolecules*. 2006;7(5):1623–1629.
45. Yang Y, Zhu X, Cui W, et al. Electrospun composite mats of poly[(D,L-lactide)-co-glycolide] and collagen with high porosity as potential scaffolds for skin tissue engineering. *Macromol Mater Eng*. 2009; 294(9):611–619.
46. Fan J, Du H, Yin Y, et al. Efficacy and safety of zotarolimus-eluting stents compared with sirolimus-eluting stents in patients undergoing percutaneous coronary interventions-a meta-analysis of randomized controlled trials. *Int J Cardiol*. 2013;167(5):2126–2133.
47. Navarese EP, Kowalewski M, Kandzari D, et al. First-generation versus second-generation drug-eluting stents in current clinical practice: updated evidence from a comprehensive meta-analysis of randomised clinical trials comprising 31 379 patients. *Open Heart*. 2014;1(1):64.
48. Zhou Q, Liao JK. Pleiotropic effects of statins: basic research and clinical perspectives. *Circ J*. 2010;74(5):818–826.
49. Kavalipati N, Shah J, Ramakrishan A, Vasnawala H. Pleiotropic effects of statins. *Indian J Endocrinol Metab*. 2015;19(5):554–562.
50. Davignon J. Beneficial cardiovascular pleiotropic effects of statins. *Circulation*. 2004;109(23 suppl 1):39–43.
51. Bedi O, Dhawan V, Sharma PL, Kumar P. Pleiotropic effects of statins: new therapeutic targets in drug design. *Naunyn Schmiedebergs Arch Pharmacol*. 2016;389(7):695–712.